A Reversible Nanoconfined Chemical Reaction

Thomas K. Nielsen,[†] Ulrike Bösenberg,[‡] Rapee Gosalawit,[‡] Martin Dornheim,[‡] Yngve Cerenius,[§] Flemming Besenbacher,[⊥] and Torben R. Jensen[†,*]

[†]Center for Energy Materials, Interdisciplinary Nanoscience Center (iNANO), and Department of Chemistry, Aarhus University, DK-8000 Aarhus, Denmark, [‡]Institute of Material Research, GKSS-Research Centre Geesthacht, D-21502 Geesthacht, Germany, [§]MAX-lab, Lund University, S-22100 Lund, Sweden, and [⊥]Interdisciplinary Nanoscience Center (iNANO) and Department of Physics and Astronomy, Aarhus University, DK-8000 Aarhus C, Denmark

ABSTRACT Hydrogen is recognized as a potential, extremely interesting energy carrier system, which can facilitate efficient utilization of unevenly distributed renewable energy. A major challenge in a future "hydrogen economy" is the development of a safe, compact, robust, and efficient means of hydrogen storage, in particular, for mobile applications. Here we report on a new concept for hydrogen storage using nanoconfined reversible chemical reactions. $LiBH_4$ and MgH_2 nanoparticles are embedded in a nanoporous carbon aerogel scaffold with pore size $D_{max} \sim 21$ nm and react during release of hydrogen and form MgB_2. The hydrogen desorption kinetics is significantly improved compared to bulk conditions, and the nanoconfined system has a high degree of reversibility and stability and possibly also improved thermodynamic properties. This new scheme of nanoconfined chemistry may have a wide range of interesting applications in the future, for example, within the merging area of chemical storage of renewable energy.

KEYWORDS: nanoconfinement · reactive hydride composite · hydrogen storage · lithium borohydride · magnesium hydride

The world today is facing increasing energy demands and simultaneously a demand for cleaner and more environmentally friendly technologies. The development of new nanomaterials is expected to have a major impact on the development of novel sustainable energy technologies.[1,2] Here we introduce a new concept, nanoconfined chemistry, as a means to improve the reversibility, stability, kinetics, and possibly also the thermodynamic properties of chemical reactions involved in reversible release and uptake of hydrogen. Hydrogen is recognized as a possible energy carrier, but its large-scale utilization is mainly hampered by insufficient hydrogen storage properties.[3,4] Lithium borohydride, $LiBH_4$, and magnesium hydride, MgH_2, have been studied intensively in the past due to their high theoretical hydrogen densities of $\rho_m = 18.5$ and 7.6 wt %, respectively.[5,6] However, the use of $LiBH_4$ as a solid-state hydrogen storage material is hampered by its unfavorable high thermal stability; that is, release of H_2 takes place at temperatures above ~400 °C and, importantly, uptake of H_2 only occurs under extreme conditions.[7] Similarly, application of the abundant and cheap metal magnesium is also impeded by unfavorable thermodynamic properties, $\Delta H_f = -75$ kJ/mol H_2 (*i.e.*, bulk MgH_2 must be heated to ~300 °C in order to release hydrogen at $p(H_2) = 1$ bar).[3,6]

Fortunately, both the kinetic and thermodynamic properties of potential hydrogen storage materials can be significantly improved by combining exothermic and endothermic chemical reactions. A more favorable total enthalpy change may be obtained by the introduction of a new dehydrogenated state which may facilitate hydrogenation.[8,9] This concept is referred to as reactive hydride composites (RHC), and it helps to preserve a high gravimetric hydrogen storage capacity.[8] An illustrative example is given by the reaction scheme depicted below.

$$2LiBH_4(l) + MgH_2(s) \rightarrow 2LiH(s) + MgB_2(s) + 4H_2(g) \quad (1)$$

Due to the formation of MgB_2, the reaction enthalpy is reduced to $\Delta H_f = -46$ kJ/mol H_2 and the hydrogen absorption occurs under more moderate conditions,[8−15] and furthermore, this reaction also has a high potential hydrogen storage capacity, $\rho_m = 11.6$ wt %. However, the reactants must be thoroughly mixed and be in intimate close contact over large surface areas in order for reaction 1 to proceed. This has previously been achieved only by mechanical top-down approaches such as extensive ball milling, which unfortunately contaminates the sample with material from balls and vial. Furthermore, metal hydride nanoparticles tend to agglomerate, sinter, and grow into

*Address correspondence to trj@chem.au.dk.

Received for review April 6, 2010 and accepted June 06, 2010.

Published online June 10, 2010.
10.1021/nn1006946

TABLE 1. Texture Parameters for the Pristine Nanoporous Carbon Aerogel Scaffold Materials

RF-aerogel	S_{BET} (m^2/g)	V_{meso} (mL/g)	V_{tot} (mL/g)	V_{micro}/V_{total}	D_{max} (nm)
X	722	1.1	1.27	0.15	22
X[a]	722	1.0	1.22	0.14	20

[a]Same batch as X but slightly different pyrolysis conditions were applied.

larger particles upon hydrogen release and uptake cycles at elevated temperatures.[1,16]

Here we introduce an alternative bottom-up approach where nanoparticles of hydrides are synthesized or melt infiltrated in a nanoporous inert scaffold material,[17−21] which has several advantages: (i) increased surface area of the reactants, (ii) nanoscale diffusion distances, and (iii) increased number of grain boundaries, which facilitate release and uptake of hydrogen and enhance reaction kinetics.[2,17−22]

RESULTS AND DISCUSSION

Infiltration of Reactive Hydride Composites. Chemically inert nanoporous resorcinol formaldehyde carbon aerogels with an average pore size of $D_{max} \sim 21$ nm and surface areas $S_{BET} \sim 722$ m^2/g were used as nanoscaffold materials in this study. The texture parameters are in good agreement with previous results for materials prepared under similar conditions (see Table 1).[17] Monoliths of aerogels (~0.4 cm^3) were infiltrated with dibutylmagnesium ($MgBu_2$) in heptane solution.[23,24] This approach offers the advantage that surface excess white crystalline $MgBu_2$ can easily be removed mechanically from the black aerogel monoliths. Furthermore, the density of $MgBu_2$ is significantly smaller as compared to the density of MgH_2, which results in "empty space" in the pores after evaporation of butane where other reactants can be infiltrated.[24] The amount of nanoconfined $MgBu_2$ can conveniently be calculated from the weight gain of the aerogel monoliths, and the quantity of magnesium hydride obtained by hydrogenation can be calculated stoichiometrically. In the following, samples of aerogel X loaded with MgH_2 are denoted X-Mg. Subsequently, lithium borohydride was melt infiltrated in monolithic samples of X-Mg in a hydrogen atmosphere, $p(H_2) = 50$ bar, in order to prevent partial decomposition of the hydrides and suppress a possible chemical reaction between the two hydrides. The amount of infiltrated $LiBH_4$ is calculated gravimetrically, and the volumetric uptake of MgH_2 and $LiBH_4$ is calculated from the total pore volume of aerogel X to be ~10 and up to 45 vol %, respectively. Experimental details about the investigated samples are listed in Table S2 in Supporting Information. The molar ratio of $LiBH_4$ and MgH_2 was adjusted to approximately 2:1 in accordance with reaction 1. The sample of aerogel loaded with MgH_2 and $LiBH_4$ is denoted X-Mg-Li. A bulk sample of $LiBH_4$ and MgH_2 (2:1) was prepared in a similar manner and used as a reference using crystalline $MgBu_2$ physically mixed with $LiBH_4$. This bulk sample is denoted Mg-Li. The direct synthesis of nanoconfined magnesium hydride, MgH_2, from crystalline dibutylmagnesium, $MgBu_2$, embedded in the aerogel and the process of melt infiltration of $LiBH_4$ was studied by *in situ* synchrotron radiation powder X-ray diffraction, SR-PXD (see Figure 1A).

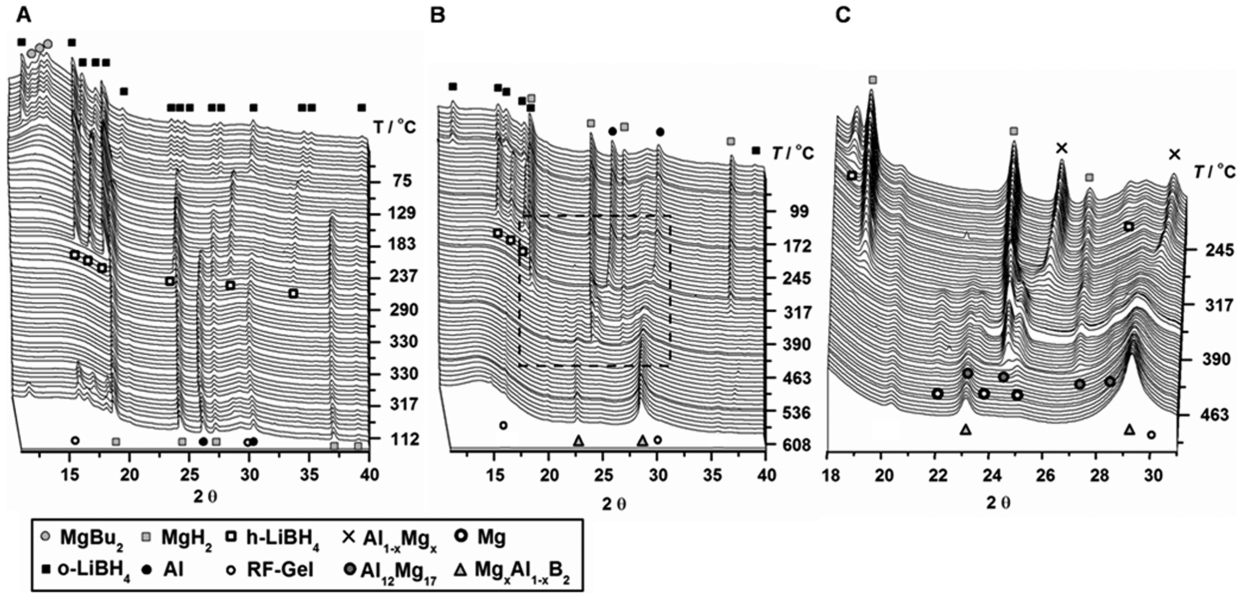

Figure 1. ***In situ*** **synchrotron radiation powder X-ray diffraction (SR-PXD) data of a sample of bulk $LiBH_4$ mixed with $MgBu_2$-embedded aerogel. (A) Synthesis of MgH_2 from $MgBu_2$ and the melt infiltration of $LiBH_4$ to obtain nanoconfined $2LiBH_4$-MgH_2 (sample X-Mg-Li). The sample was initially heated from room temperature to 330 °C and kept at a fixed temperature of 330 °C for 25 min and subsequently cooled to room temperature (heating and cooling rates 5.4 and 20.0 °C/min) under a hydrogen pressure of $p(H_2) = 50$ bar (A). The experiment presented in panel A was continued, heating the sample (X-Mg-Li) from room temperature to 614 °C (heating rate 7.1 °C/min) under a hydrogen pressure of $p(H_2) = 5$ bar (B). This *in situ* SR-PXD data in panel B illustrates the first hydrogen desorption from sample X-Mg-Li. (C) Enlargement of a selected area (the square) shown in panel B ($\lambda = 1.072$ Å).**

Diffraction from crystalline $MgBu_2$ is observed in the temperature range from room temperature to 140 °C, and the direct conversion of $MgBu_2$ to MgH_2 occurs within a few minutes at 140−150 °C (heating rate 5.4 °C/min, $p(H_2) = 50$ bar). Lithium borohydride transforms from an orthorhombic to a hexagonal polymorph at $T \sim 112$ °C, and the diffraction disappears in the temperature range of 272−277 °C due to melting and reappears upon cooling. After melt infiltration, the $LiBH_4$ diffraction peaks are broader; that is, an increase in fwhm parameters from 0.23 to 0.33° is observed (see Figure S1 in Supporting Information), which indicates a reduction of the average crystallite size and maybe increased stress and strain in the diminished particles of $LiBH_4$ due to nanoconfinement. However, crystal growth is expected upon melting and cooling $LiBH_4$, but the presence of a nanoporous scaffold clearly introduces melt infiltration and nanoconfinement. We observe no indications of any chemical reactions between the aerogel scaffold material, MgH_2, Mg, and $LiBH_4$ due to the elevated hydrogen pressures of $p(H_2) = 50$ bar. However, diffraction from aluminum appears at $T = 253$ °C due to reduction of triethylaluminum present in the used $MgBu_2$ solution.

Nanoconfined Chemical Reactions. The hydrogenated sample X-Mg-Li prepared *in situ* (Figure 1A) was used in a continuation of the experiment for a study of the dehydrogenation mechanism displayed in Figure 1B. The polymorphic phase transition and subsequent melting of nanoconfined $LiBH_4$ is again observed. Diffraction from MgH_2 fades out during formation of an intermediate phase, $Al_{1-x}Mg_x$. Dissolution of magnesium in solid aluminum is observed as an expansion of the aluminum unit cell. Diffraction from $Al_{1-x}Mg_x$ and MgH_2 is observed to vanish simultaneously at $T \sim 365$ °C, where Mg and $Al_{12}Mg_{17}$ crystallize (see Figure 1B,C), in agreement with previous studies.[25] Diffraction from Mg and $Al_{12}Mg_{17}$ fades simultaneously with the formation of an aluminum containing magnesium boride phase, $Mg_{1-x}Al_xB_2$ (MgB_2 and AlB_2 are isomorphous). The formation of $MgAlB_4$ has been suggested in previous studies of the system $4LiBH_4$-MgH_2-Al.[26] Lithium hydride has diffraction peaks overlapping with both the MgB_2 and Al. Furthermore, the experiment illustrated in Figure 1 was repeated with another sample from the same batch studying also the first hydrogen absorption, which is shown in Figure S3 in Supporting Information. Diffraction from Al and MgH_2 appears at $T \sim 330$ °C and $p(H_2) = 120-150$ bar with a simultaneous drop in diffracted intensity from the $Mg_{1-x}Al_xB_2$ phase.

Hydrogen desorption from nanoconfined carbon aerogel $2LiBH_4$-MgH_2 composite and bulk $2LiBH_4$-MgH_2 was studied by simultaneous differential scanning calorimetry, thermogravimetric analysis, and mass spectrometry (DSC/TGA/MS) under the exact same physical conditions, which provided valuable insight into the hydrogen desorption mechanism (see Figure 2).

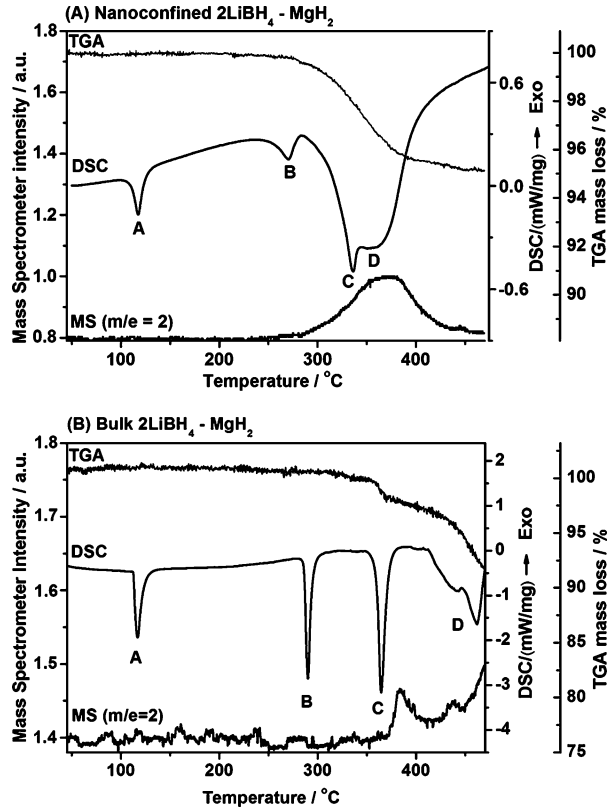

Figure 2. Simultaneous differential scanning calorimetry (DSC), thermogravimetric analysis (TGA), and mass spectrometry (MS) showing the hydrogen release reactions from nanoconfined and bulk $2LiBH_4$-MgH_2. (A) Nanoconfined $2LiBH_4$-MgH_2 (sample X-Mg-Li) and (B) bulk $2LiBH_4$-MgH_2 (sample Mg-Li). Both samples were heated from room temperature to 470 °C (heating rate 5 °C/min, argon flow 50 mL/min). Two cycles of hydrogen release and uptake in magnesium were conducted prior to addition of $LiBH_4$ in the samples.

The DSC analysis reveals four distinct endothermic desorption peaks denoted A, B, C, and D for both samples but observed at significantly different temperatures. Peaks A and B are observed at 113 and 267 °C and at 117 and 290 °C for the nanoconfined and the bulk hydride composite, respectively (peak temperature values are given). These events, A and B, are assigned to the orthorhombic to hexagonal transformation and the melting of $LiBH_4$, respectively. Interestingly, the peak temperature for melting of $LiBH_4$ is shifted significantly to a lower value ($\Delta T = 23$ °C) for the nanoconfined hydride composite as compared to the bulk sample. This is consistent with a previous observation for $LiBH_4$ confined within small pores.[17]

The thermal events C and D are observed at 332 and ~351 °C and at 364 and ~462 °C for the nanoconfined and the bulk composite hydrides, respectively. Events C and D reveal a mass loss from the hydride composites in the form of hydrogen gas and are assigned to the dehydrogenation of MgH_2 and $LiBH_4$, respectively. There was no indication of any release of borane gases. The nanoconfined hydride sample releases 4.7 wt % hydrogen in the temperature range of 260 to 470 °C, which is in good agreement with the calculated

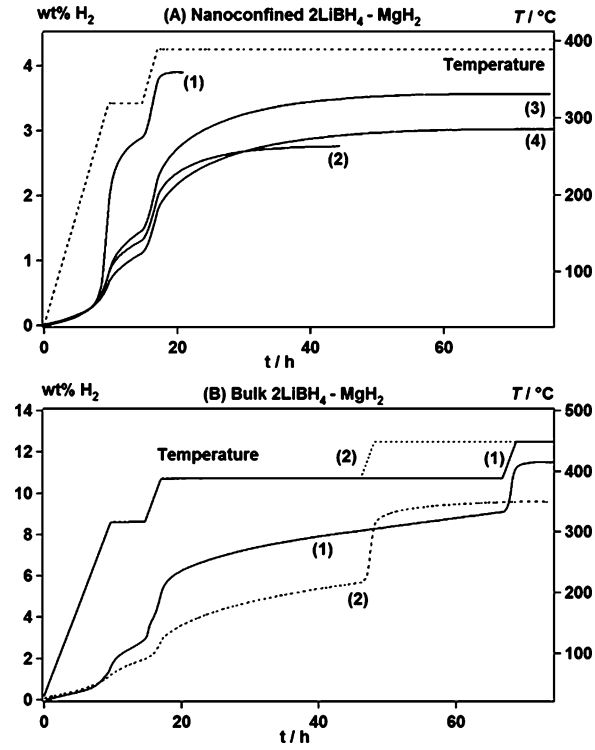

Figure 3. Sieverts' measurements showing hydrogen desorption profiles for nanoconfined and bulk $2LiBH_4$-MgH_2. (A) Melt infiltration of $LiBH_4$ in nanoconfined magnesium hydride was performed during the first hydrogen desorption to obtain sample X-Mg-Li. Hydrogen desorption was performed at fixed temperatures of 320 and 390 °C. (B) Bulk $2LiBH_4$-MgH_2 (sample Mg-Li) desorbed at fixed temperatures of 320, 390, and 450 °C (heating rates 0.5 °C/min and $p(H_2) = 2$ bar).

mass loss of 4.3 wt % H_2 based on the measured MgH_2 and $LiBH_4$ uptake (see Table S2 in Supporting Information) and the observed intensity of the H_2 signal ($m/e = 2$) in the mass spectrometer. Peak D for the bulk sample of $2LiBH_4$-MgH_2 also includes a minor event at ~440 °C in addition to the major event at ~462 °C. Pure $LiBH_4$ is known to release hydrogen in several steps.[5] The bulk sample releases a total of 9.2 wt % H_2 in the temperature range of 260 to 470 °C. Hydrogen desorption is clearly not completed at 470 °C and does not reach the calculated mass loss of 11.5 wt % H_2. The results

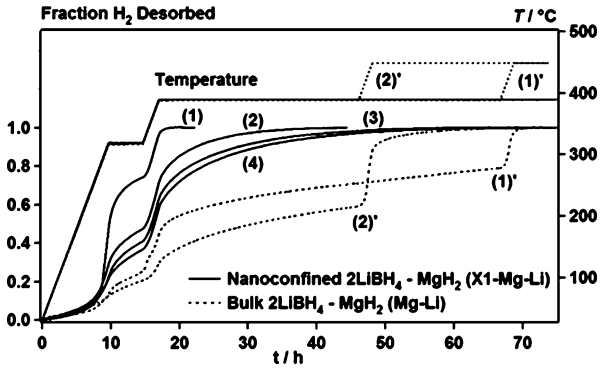

Figure 4. Normalized Sieverts' hydrogen desorption profiles (data from Figure 3A,B). The hydrogen release kinetics from nanoconfined (solid line) and bulk $2LiBH_4$-MgH_2 (dashed line) is compared.

for bulk $2LiBH_4$-MgH_2 (Figure 2B) compares well with previously reported data for similar ball-milled samples revealing peaks C and D, temperatures in the DSC profiles of 346, 414, and 443 °C (peak D was split up), and onset temperature for hydrogen release at ~300 °C.[10] The onset temperatures for hydrogen release for the nanoconfined and the bulk sample are ~260 and 350 °C, respectively. Figure 2A,B clearly shows that nanoconfinement of $2LiBH_4$-MgH_2 significantly improves hydrogen desorption kinetics; that is, the onset temperature for hydrogen release is reduced by 90 °C according to TGA, and peaks C and D temperatures in the DSC profiles are reduced by 32 and 89−111 °C, respectively. These results may also indicate thermodynamic improvements; however, this needs further investigations. A significant reduction of hydrogen release temperatures has previously been observed for the individually nanoconfined hydrides MgH_2 and $LiBH_4$.[24,27] Therefore, the results depicted in Figure 2A clearly illustrate that both hydrides are nanoconfined inside the nanoporous aerogel scaffold in the present study. Furthermore, the results also suggest that the mechanism for hydrogen release for the nanoconfined reactive hydride composite has been altered as compared to the bulk system.

Kinetic Properties and Reversibility. The reversible hydrogen storage capacity and desorption kinetics of the nanoconfined and bulk $2LiBH_4$-MgH_2 composite were studied by the Sieverts' method. A total of four hydrogen release and uptake cycles were measured, and the desorption profiles are depicted in Figure 3A. The nanoconfined sample X-Mg-Li desorbed 3.9 wt % H_2 at 390 °C, $p(H_2) = 2$ bar after 20 h, in accordance with the calculated hydrogen content of 3.9 wt % H_2 (see Table S2 in Supporting Information). The first hydrogen absorption was performed under relatively mild conditions, $T = 370$ °C, $p(H_2) = 70$ bar for 35 h, and therefore, the second desorption released only 2.8 wt % H_2. A more complete second hydrogenation reaction was obtained at 390 °C, ~98 bar H_2 for 68 h; therefore, the third desorption released 3.6 wt % H_2 (see Figure 3A). The third hydrogenation was performed at 390 °C, ~93 bar H_2 for 88 h, and the fourth desorption released 3.0 wt % H_2. These results reveal that nanoconfined $2LiBH_4$-MgH_2 stores hydrogen reversibly and that the storage capacity depends on the conditions for hydrogen uptake (in this case 74% of the capacity is preserved over four cycles). For comparison of reversibility and storage capacity, the bulk $2LiBH_4$-MgH_2 sample (Mg-Li) was also investigated using the Sieverts' method.

Clearly, higher temperatures are needed in order to release and absorb hydrogen (see Figure 3B). The first hydrogen desorption from sample Mg-Li released 11.5 wt % H_2, in accordance with reaction 1 (see also Table S2), but was achieved under more harsh conditions, with temperatures up to 450 °C, $p(H_2) = 2$ bar for 74 h, as compared to the nanoconfined $2LiBH_4$-MgH_2. Hydrogenation was performed at $T = 450$ °C, $p(H_2) = 91$ bar

for 54 h, and the second desorption released 9.6 wt % hydrogen. The physical conditions for hydrogen uptake may be further optimized to achieve faster absorption.

In Figure 4, normalized hydrogen desorption profiles are utilized to compare the kinetic properties of nanoconfined and bulk $2LiBH_4$-MgH_2 samples. The hydrogen desorption rate is significantly higher for the nanoconfined sample as compared to bulk $2LiBH_4$-MgH_2. For both samples, the hydrogen desorption rate decreases during cycling with hydrogen release and uptake. We find that 74% of the total hydrogen content in nanoconfined $2LiBH_4$-MgH_2 is released at $T \leq 320$ °C after 15 h, for the bulk sample only 26% is released, which clearly demonstrates a considerable improvement in the hydrogen desorption kinetics for the nanoconfined $2LiBH_4$-MgH_2 and possibly also of the thermodynamic properties. Furthermore, Figure 4 shows that the hydrogen desorption kinetics from the nanoconfined $2LiBH_4$-MgH_2 has been considerably improved as compared to the bulk sample even after four hydrogen release and uptake cycles. According to the Sieverts' measurements, ~92% of the initial hydrogen storage capacity is available through three cycles, which is significantly higher than that reported for the nanoconfined $LiBH_4$ without MgH_2 (*i.e.*, ~40% over three cycles in 25 nm aerogel).[17] Furthermore, the measured reversible hydrogen storage capacity of ~4 wt % for nanoconfined $2LiBH_4$-MgH_2 is significantly higher than that for nanoconfined MgH_2 without $LiBH_4$ (*i.e.*, ~1.40 wt % in 22 nm aerogel).[24] Furthermore, considering that the nanoconfined $2LiBH_4$-MgH_2 occupies only ~55 vol % of the accessible pore volume (see Table S2 in Supporting Information), the gravimetric hydrogen content may be increased even further by utilizing more impregnation cycles of the respective hydrides.

CONCLUSIONS

This work shows that nanoconfined $2LiBH_4$-MgH_2 possesses a high degree of reversible stability, improved hydrogen desorption kinetics, and possibly also improved thermodynamic properties. The nanoconfined hydride has a significant hydrogen storage potential, considering that only ~55 vol % of the free accessible pore volume in the nanoporous scaffold material is utilized. The physical and chemical conditions for hydrogen release and uptake may also be further optimized. Thus, nanoconfinement may significantly improve the properties of reactive hydride composites in the future. Nanoconfinement may influence or alter the reaction mechanism for hydrogen release and uptake. Furthermore, the concept of nanoconfined chemical reactions may develop to become an important tool within the emerging area of nanotechnology for the improvement of the properties and reaction yield of a wide range of chemical reactions.

METHODS

Sample Preparation. The resorcinol formaldehyde aerogels, denoted RF-gels in the following, were prepared and characterized according to previously published procedures.[17,24,28] However, two different batches of RF-gel X are used. The pyrolysis time of batch X was 6 h at 800 °C and 3 h for X* in a flow of nitrogen. Selected gels were activated at 400 °C in vacuum for several hours in order to remove moisture and gases from the porous structure.

Monoliths of RF-gel (*ca.* 0.4 cm^3) X or X* (see Table 1) were covered with excess amounts of a solution consisting of 1 M dibutylmagnesium ($MgBu_2$) in heptane (Aldrich). This procedure was performed under a purified argon atmosphere in a glovebox. The gels were left to dry for several days, and as the heptane evaporated, the dibutylmagnesium crystallized in the pores. The monoliths of gels were easily distinguished and separated from the excess amount of dibutylmagnesium. White crystalline dibutylmagnesium deposited on the surface of the rigid aerogel material was carefully removed mechanically. The uptake of magnesium hydride in the RF-gels was calculated by measuring the mass of the aerogels before and after loading them with $MgBu_2$ (see Supporting Information Table S2). Samples of RF-gels loaded with both MgH_2 and $LiBH_4$ were prepared in two different ways.

The samples to be studied by synchrotron radiation powder X-ray diffraction (SR-PXD) experiments and Sieverts' measurements were prepared by grinding monoliths of aerogel loaded with dibutylmagnesium together with $LiBH_4$ (>90%, Aldrich), obtaining a powder. $LiBH_4$ is expected to infiltrate the nanoporous scaffold material by melt infiltration during the measurements when the temperature exceeds the melting point, $T_m = 275$ °C. The molar ratio of MgH_2 and $LiBH_4$ in the mixture was approximately 1:2. A sample of crystalline $MgBu_2$ physically mixed with $LiBH_4$ (without aerogel) was also prepared and used as a reference.

Samples to be studied by DSC/TG/MS experiments were prepared by a different route. Monoliths of aerogel loaded with $MgBu_2$ were first hydrogenated, forming nanoconfined MgH_2. Dibutylmagnesium reacts with hydrogen to form magnesium hydride and butane at a temperature of 170 °C and a hydrogen pressure of $p(H_2) = 50$ bar. The samples of aerogel-MgH_2 composite were then cycled twice with hydrogen release and uptake at a fixed temperature of 380 °C and hydrogen pressures of 10^{-2} or 90 bar. Subsequently, the samples were placed in a stainless steel cylinder together with $LiBH_4$. Nanoconfined $LiBH_4$ was then obtained by melt infiltration at 300 °C and a hydrogen pressure of $p(H_2) = 50$ bar. A molar ratio of MgH_2 and $LiBH_4$ close to 1:2 was obtained by adding adequate amounts of $LiBH_4$ (see Table S2). The uptake of $LiBH_4$ was calculated by measuring the mass of the aerogel-MgH_2 composites before and after melt infiltration (see Table S2). A sample of magnesium hydride was prepared by hydrogenation of crystalline dibutylmagnesium (without aerogel) and cycling twice with hydrogen release and uptake using the same procedure as described above. The freshly prepared magnesium hydride was physically mixed with $LiBH_4$. This sample is denoted Mg-Li and was used as a reference. These procedures were carried out under inert conditions in either a PCTpro 2000 apparatus from Hy-energy or a custom-made manual hydrogenation station. All handling of samples was performed under a purified argon atmosphere in a glovebox.

Sieverts' Measurements. The cyclic stability of MgH_2 and $LiBH_4$ embedded in aerogel was studied by Sieverts' measurements (PCTpro 2000), and a total of four hydrogen uptake and release cycles were performed. The ground mixture of aerogel loaded with crystalline dibutylmagnesium and $LiBH_4$ was transferred to an autoclave and sealed under argon in a glovebox. The estimated quantity of MgH_2 in the mixture was 23.2 mg, and the amount of $LiBH_4$ was 38.3 mg. The autoclave was attached to

the PCTpro 2000 apparatus, and the synthesis of MgH_2 was performed under similar conditions as described above. Hydrogen desorption data were collected in the temperature range from room temperature to 390 °C and with the temperature kept fixed at 320 °C for 5 h. The heating rate was 0.5 °C/min. Hydrogen absorption was performed at $p(H_2) = 50-100$ bar in the temperature range of 370−390 °C for several days. A sample of dibutylmagnesium physically mixed with $LiBH_4$ was used for reference, and similar conditions were applied. However, in order to fully release the hydrogen from this sample, it was necessary to heat it to 450 °C.

Thermal Analysis. Differential scanning calorimetry and thermogravimetric (TG) measurements were performed simultaneously in a Netzsch STA 409 C in an argon atmosphere with the entire apparatus placed in a dedicated glovebox under a purified argon atmosphere. One monolith of aerogel loaded with nanoconfined MgH_2 and $LiBH_4$ was transferred to the sample holder and heated from room temperature to 475 °C. The heating rate was 5 °C/min, and a continuous argon flow of 50 mL/min was applied. The concentration of H_2, B_2H_6, and Ar in the exhaust gas was continuously recorded by a Hiden HPR-20 QIC mass spectrometer.

***In Situ* SR-PXD Measurements.** *In situ* synchrotron radiation powder X-ray diffraction (SR-PXD) data were collected at beamline I711 at MAX-lab, Lund, Sweden. The ground mixture of aerogel loaded with crystalline dibutylmagnesium and $LiBH_4$ was placed in a sapphire capillary tube with an inner diameter of 0.79 mm. A *ca.* 10 mm long powder sample was mounted in the tube and placed in an airtight sample holder. The sample holder was moved from the glovebox to the diffractometer under inert conditions. The selected X-ray wavelength was $\lambda = 1.072$ Å, and *in situ* SR-PXD data were collected using a MAR CCD detector. The sample was heated in the temperature range from room temperature to 614 °C with heating rates from 5 to 15 °C/min, and the hydrogen pressure was varied from 10^{-2} to 150 bar.

Acknowledgment. The work was supported by the Danish National Research Foundation (Centre for Materials Crystallography), the Danish Strategic Research Council (Centre for Energy Materials), and the Danish Research Council for Nature and Universe (Danscatt). We are grateful to the Carlsberg Foundation.

Supporting Information Available: Experimental details, *in situ* SR-PXD data, gauss fits, and evaluation of crystalline grain size. This material is available free of charge *via* the Internet at http://pubs.acs.org.

REFERENCES AND NOTES

1. Bérube, V.; Radtke, G.; Desselhaus, M.; Chen, G. Size Effects on the Hydrogen Storage Properties of Nanostructured Metal Hydrides: A Review. *Int. J. Energy Res.* **2007**, *31*, 637–663.
2. Bérube, V.; Chen, G.; Dresselhaus, M. S. Impact of Nanostructuring on the Enthalpy of Formation of Metal Hydrides. *Int. J. Hydrogen Energy* **2008**, *33*, 4122–4131.
3. Schlapbach, L.; Züttel, A. Hydrogen-Storage Materials for Mobile Applications. *Nature* **2001**, *414*, 353–358.
4. Eberle, U.; Felderhoff, M.; Schüth, F. Chemical and Physical Solutions for Hydrogen Storage. *Angew. Chem., Int. Ed.* **2009**, *48*, 6608–6630.
5. Orimo, S.; Nakamori, Y.; Eliseo, J. R.; Züttel, A.; Jensen, C. M. Complex Hydrides for Hydrogen Storage. *Chem. Rev.* **2007**, *107*, 4111–4132.
6. Dornheim, M.; Eigen, N.; Barkhordarian, G.; Klassen, T.; Bormann, R. Tailoring Hydrogen Storage Materials towards Application. *Adv. Eng. Mater.* **2006**, *8*, 377–385.
7. Mauron, P.; Buchter, F.; Friedrichs, O.; Remhof, A.; Bielmann, M.; Zwicky, C. N.; Züttel, A. Stability and Reversibility of $LiBH_4$. *J. Phys. Chem. B* **2008**, *112*, 906–910.
8. Barkhordarian, G.; Klassen, T.; Dornheim, M.; Bormann, R. Unexpected Kinetic Effect of MgB_2 in Reactive Hydride Composites Containing Complex Borohydrides. *J. Alloys Compd.* **2007**, *440*, L18–L21.
9. Vajo, J. J.; Skeith, L. S.; Mertens, F. Reversible Storage of Hydrogen in Destabilized $LiBH_4$. *J. Phys. Chem. B* **2005**, *109*, 3719–3722.
10. Bösenberg, U.; Doppiu, D.; Mosegaard, L.; Barkhordarian, G.; Eigen, N.; Borgschulte, A.; Jensen, T. R.; Cerenius, Y.; Gutfleisch, O.; Klassen, T.; *et al.* Hydrogen Sorption of MgH_2-$LiBH_4$ Composites. *Acta Mater.* **2007**, *55*, 3951–3958.
11. Pinkerton, F. E.; Meyer, M. S.; Meisner, G. P.; Balogh, M. P.; Vajo, J. J. Phase Boundaries and Reversibility of $LiBH_4$/MgH_2 Hydrogen Storage Material. *J. Phys. Chem. C* **2007**, *111*, 12881–12885.
12. Walker, G. S.; Grant, D. M.; Price, T. C.; Yu, X.; Legrand, L. High Capacity Multicomponent Hydrogen Storage Materials: Investigation of the Effect of Stoichiometry and Decomposition Conditions on the Cycling Behaviour of $LiBH_4$-MgH_2. *J. Power Sources* **2009**, *194*, 1128–1134.
13. Bösenberg, U.; Kim, J. K.; Gosslar, D.; Eigen, N.; Jensen, T. R.; von Colbe, J. M. B.; Zhou, Y.; Dahms, M.; Kim, D. H.; Günther, R.; *et al.* Role of Additives in $LiBH_4$-MgH_2 Reactive Hydride Composites for Sorption Kinetics. *Acta Mater.* **2010**, *58*, 3381–3389.
14. Wan, X.; Markmaitree, T.; Osborn, W.; Shaw, L. L. Nanoengineering-Enabled Solid-State Hydrogen Uptake and Release in the $LiBH_4$ Plus MgH_2 System. *J. Phys. Chem. C* **2008**, *112*, 18232–18243.
15. Cho, Y. W.; Shim, J.-H.; Lee, B.-J. Thermal Destabilization of Binary and Complex Metal Hydrides by Chemical Reaction: A Thermodynamic Analysis. *CALPHAD* **2006**, *30*, 65–69.
16. Gertsman, V. Y.; Birringer, B. On the Room-Temperature Growth in Nanocrystalline Copper. *Scripta Metall. Mater.* **1994**, *30*, 577–581.
17. Gross, A.; Vajo, J. J.; Atta, S. L. V.; Olson, G. L. Enhanced Hydrogen Storage Kinetics of $LiBH_4$ in Nanoporous Carbon Scaffolds. *J. Phys. Chem. C* **2008**, *112*, 5651–5657.
18. Gutowska, A.; Li, L.; Shin, Y.; Wang, M. C.; Li, S. X.; Linehan, J. C.; Smith, R. S.; Kay, B. D.; Schmid, B.; Shaw, W.; *et al.* Nanoscaffold Mediates Hydrogen Release and the Reactivity of Ammonia Borane. *Angew. Chem., Int. Ed.* **2005**, *44*, 3578–3582.
19. Kim, H.; Karkamkar, A.; Autrey, T.; Chupas, P.; Proffen, T. Determination of Structure and Phase Transition of Light Element Nanocomposites in Mesoporous Silica: Case Study of NH_3BH_3 in MCM-41. *J. Am. Chem. Soc.* **2009**, *131*, 13749–13755.
20. Sartori, S.; Knudsen, K. D.; Zhao-Karger, Z.; Bardajj, E. G.; Fichtner, M.; Hauback, B. Small-Angle Scattering Investigations of Mg-Borohydride Infiltrated in Activated Carbon. *Nanotechnology* **2009**, *20*, 505702.
21. Baldé, C. P.; Hereijgers, B. P. C.; Bitter, J. H.; de Jong, K. P. Facilitated Hydrogen Storage in $NaAlH_4$ Supported on Carbon Nanofibers. *Angew. Chem., Int. Ed.* **2006**, *45*, 3501–3503.
22. Zaluski, L.; Zaluska, A.; Ström-Olsen, J. O. Nanocrystalline Metal Hydrides. *J. Alloys Compd.* **1997**, *253−254*, 70–79.
23. Zhang, S.; Gross, A. F.; Atta, S. L. V.; Lopez, M.; Liu, P.; Ahn, C. C.; Vajo, J. J.; Jensen, C. M. The Synthesis and Hydrogen Storage Properties of a MgH_2 Incorporated Carbon Aerogel Scaffold. *Nanotechnology* **2009**, *20*, 204027.
24. Nielsen, T. K.; Manickam, K.; Hirscher, M.; Besenbacher, F.; Jensen, T. R. Confinement of MgH_2 Nanoclusters within Nanoporous Aerogel Scaffold Materials. *ACS Nano* **2009**, *3*, 3521–3528.
25. Andreasen, A.; Sørensen, M. B.; Burkarl, R.; Møller, B.; Molenbroek, A. M.; Pedersen, A. S.; Andreasen, J. W.; Nielsen, M. M.; Jensen, T. R. Interaction of Hydrogen with an Mg-Al Alloy. *J. Alloys Compd.* **2005**, *404−406*, 323–326.
26. Zhang, Y.; Tian, Q.; Chu, H.; Zhang, J.; Sun, L.; Sun, J.; Wen, Z. Hydrogen De/Resorption Properties of the $LiBH_4$-MgH_2-Al System. *J. Phys. Chem. C* **2009**, *113*, 21964–21969.
27. Cahen, S.; Eymery, J. B.; Janot, R.; Tarascon, J. M. Improvement of the $LiBH_4$ Hydrogen Desorption by Inclusion into Mesoporous Carbons. *J. Power Sources* **2009**, *189*, 902–908.
28. Li, W.-C.; Lu, A.-H.; Weidenthaler, C.; Schüth, F. Hard-Templating Pathway To Create Mesoporous Magnesium Oxide. *Chem. Mater.* **2004**, *16*, 5676–5681.